XIII.1

Domino Structures as a local accommodation process in shear zones

Index

XIII.1.1. Introduction 255

XIII.1.2. Geological Setting 256

XIII.1.2.1. The Porto-Tomar-Ferreira do Alentejo Shear Zone 257

XIII.1.2.2. Variscan Deformation in Abrantes; Geometry and Kinematics 258

XIII.1.2.3. D_2 Variscan Deformation in Abrantes; Geodynamical Evolution 259

XIII.1.3. The Abrantes Local Strike-Slip Domino 260

XIII.1.3.1. Geometrical and Kinematical Characterization 262

XIII.1.3.2. Rotational and Translational Characterization 265

XIII.1.3.2.1. The Initial Angles; a Geostatistical Approach 266

XIII.1.3.2.2. Rotation and Translation of Dominos Blocks 269

XIII.1.3.2.3. Quantitative approach to Deformation 271

XIII.1.4. Dynamic Processes and Genesis of Domino Structures; Discussion 274

XIII.1.5. Final Remarks 276

XIII.1.1. Introduction

Domino (sometimes called bookshelf) structures have been described from low to high-grade metamorphic rocks, although they are commonly developed in brittle to ductile-brittle deformation regimes (Mandl, 2000; Ribeiro, 2002; Goscombe and Passchier, 2003; Figueiredo *et al*., 2004), obeying to Coulomb criterion for failure (Jaeger and Cook, 1981). These structure are characterized by block rotation, which are delimited by one dominant shear/fracture orientation (e.g. Mandl 2000; Nixon et al., 2011; Fossen, 2010).

Dominos can be used as a shear sense criteria (Passchier *et al.*, 1990; Mandl, 2000; Goscombe and Passchier, 2003; Goscombe et al., 2004; Passchier and Trouw, 2005; Fossen, 2010), helping the knowledge of the shear zones dynamics. These structures are described in all geodynamic settings (e.g. Wernicke and Burchfiel, 1982; Mandl, 1984; 1987; Cowan, 1986; Axen, 1988; La Femina et al., 2002) and from the microscale to orogenic scale (e.g. Ribeiro, 2002; La Femina et al., 2002; Goscombe et al., 2004; Nixon et al., 2011; Dias et al, 2016a). The careful analysis of its geometry and kinematics, as well its genesis mechanism, becomes essential to a correct dynamic interpretation of shear zones.

The dominos could have either antithetic or synthetic rotation relative to the main shear (e.g. Goscombe and Passchier, 2003; Scholz *et al.*, 2010; Dabrowski and Grasemann, 2014). This is a major constrain for their use as kinematic criteria, unless they are coupled with other structures. If this is not a major problem in extensional regimes, because rotation of dominos generally occurs antithetically to the main shear planes, in this cases a low angle ductile decollement (e.g. Wernicke and Burchfiel, 1982; Mandl, 1987; Axen, 1988; Fossen and Hesthammer, 1998; Bahroudi et al., 2003; Karlstrom et al, 2010), it strongly limits their use as kinematical criteria in strike-slip environments where both types of block rotations are described (e.g. Cowan et al., 1986; Mandl, 2000; Goscombe and Passchier, 2003; Goscombe *et al.*, 2004; Nixon *et al*., 2011; Dabrowski and Grasemann, 2014). In such cases, the block rotation (synthetic or antithetic) seems to be constrained by several factors such as flow type, rheological contrast, initial angle of the previous foliation to the main shear zone, existence of previous anisotropies bounding blocks or the shape of the block (e.g. Mandal *et al.*, 2000; Goscombe and Passchier, 2003; Dabrowski and Grasemann, 2014). However, analogue experiments (Karmakar and Mandal, 1989; Mandal and Khan, 1991; Mandal *et al.*, 2007) indicate that the orientation and the spacing of fractures in the brittle layers are the main factors that control the kinematics of domino structures. Mandl (2000) refers that in brittle domino structures, the sense of rotation depends on the nature of the planar structures that limits the blocks: when the blocks are bounded by R 'or P' shears, the synthetic rotations tend to prevail.

This work shows as a detailed geometrical and kinematical analysis of a domino domains could help to constrain some of the mechanisms to domino formation. Such approach is based on simple and easily measurable linear and angular geometric parameters. The use of this methodology in a small and well outcropping sector in relation to one of the most important Iberian Variscan Structure, the Porto-Tomar-Ferreira do Alentejo dextral shear zone (PTFASZ; *e.g.* Ribeiro *et al.*, 2007), prove to be useful in highlighting its geodynamical evolution.

XIII.1.2. Geological Setting

The Variscan chain is part of a major orogenic belt, with 1000 km wide and 8000 km of extension long from Caucasus to Appalaches and Ouachita mountains (Matte, 2001; Nance *et al.*, 2010; 2012). This orogenic belt was formed between 480-250 Ma, due to a complex collision process between three major plates: Gondwana, Laurentia and Baltica (Matte, 2001; Ribeiro *et al.*, 2007; Nance *et al.,* 2010; 2012; Dias *et al.*, 2016b). The Variscides, with rocks ranging from Neoproterozoic to upper Palaeozoic, are well exposed in the Iberian Peninsula in the so called Iberian Massif (Fig. 1A). In the older rocks of this Massif the Variscan deformation overprints previous tectonic events (*e.g.* Ribeiro *et al.,* 2007; 2009).

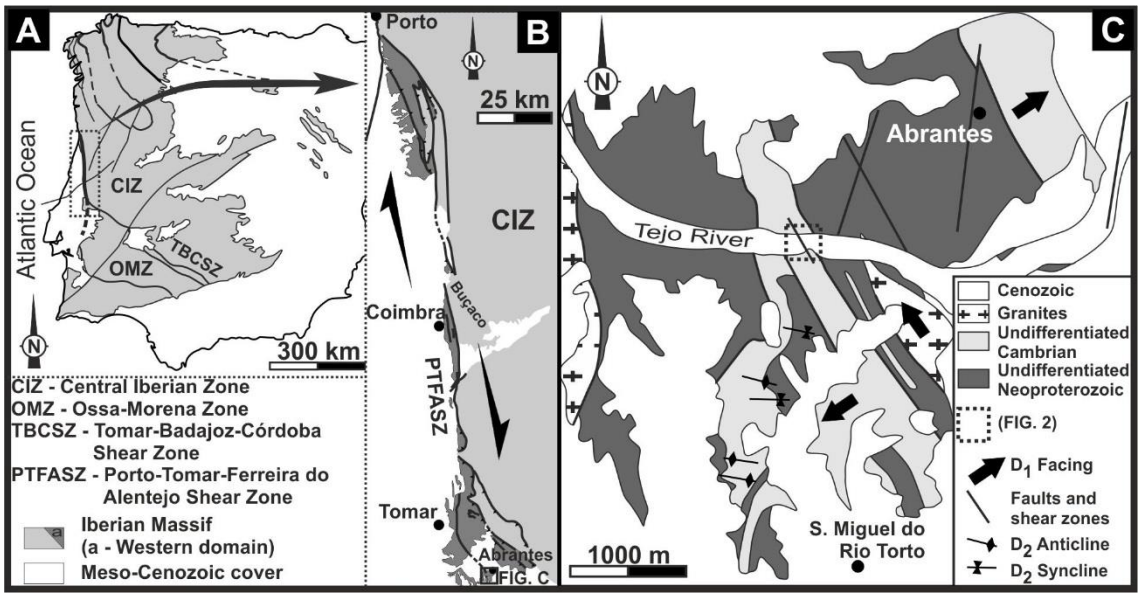

Figure 1 – The Abrantes sector in the context of the Iberian Variscides:

A – Major features of the pre-Mesozoic domains (in grey; adapted from Ribeiro et al., 1979; 2007; 2013; Dias et al, 2016b);

B – General pattern of Porto-Tomar-Ferreira do Alentejo Shear Zone (PTFASZ);

C – Geological sketch of Abrantes region.

The Iberian Massif was initially subdivided in several zones by Lotze (1945) based on stratigraphic, paleogeographic, tectonic, magmatic and metamorphic features. Subsequently, several authors (*e.g.* Julivert *et al.*, 1974; Ribeiro *et al.*, 1979) reinterpreted such zones and their boundaries, although preserving the general pattern. Since then, the Central Iberian Zone (CIZ) has been considered the internal domain of the Iberian Variscides. The boundary of this zone is marked by two first-order structures (Ribeiro *et al.*, 2007; Romão et al., 2014): the sinistral NW-SE Tomar-Badajoz-Cordova Shear Zone (TBCSZ; Fig. 1A) at South and Southwest, and the dextral NNW-SSE to N-S Porto-Tomar-Ferreira do Alentejo Shear Zone (PTFASZ; Fig. 1B) in its Western domain.

XIII.1.2.1. The Porto-Tomar-Ferreira do Alentejo Shear Zone

The PTFASZ is a lithospheric scale structure (Iglesias and Ribeiro, 1981; Shelley and Bossière, 2000; Chaminé *et al.*, 2003; Ribeiro *et al.*, 2007; Dias et al., 2016b), with a total length of, at least, 400 km. Most of the observed structures are compatible with a progressive dextral strike-slip deformation under a ductile to brittle-ductile regimes (Lefort and Ribeiro, 1980; Iglesias and Ribeiro, 1981; Ribeiro *et al.*, 2007; 2009; Pereira *et al.*, 2010; Romão *et al.*, 2014; Moreira et al., 2016). Nevertheless, despite the general agreement concerning its kinematics, the geodynamic interpretation of this structure is still a debatable subject.

The PTFASZ, sometimes considered a major dextral transform fault (Ribeiro *et al.*, 2007; 2009), put the CIZ in contact with a western domain, either considered as the Ossa-Morena paleogeographic zone (Chaminé et al., 2003; Pereira et al., 2010) or a small terrain called Finisterra (Ribeiro et al., 2007; 2013; Romão et al., 2014; Moreira et al., 2016). However, the age of this major shear zone is debatable. Although an important dextral shearing during Upper Carboniferous is accepted in all models (e.g. Ribeiro et al., 2007; Pereira et al., 2010; Moreira et al 2014; 2016), some authors (Ribeiro *et al.*, 2007; 2009; Romão *et al.*, 2013; 2014; Dias *et al.*, 2016b) considered that it was already active, with a similar kinematics, at least since Lower Devonian during the D_1 Variscan tectonic event. This conclusion is also supported by the pattern of finite strain ellipsoids in the Ordovician Quartzites of the Buçaco region (Fig. 1B; Dias and Ribeiro, 1993; 1994) and by recent geological mapping (Moreira, 2012; Romão *et al.,* 2013; 2014; Moreira et al., 2016), which shows that the interaction between PTFASZ and TBCSZ prevails during most of the Variscan deformation in Iberia.

The evidences for a strong Upper Cambrian compressive deformation in the Southwest domains of CIZ, coupled with its geometry and kinematics, indicate that PTFASZ could have been a dextral intraplate transform before the Variscan cycle (Lefort and Ribeiro, 1980; Romão *et al.*, 2005; 2013).

Nevertheless, Pereira *et al.* (2010) sustain that there is no evidence to consider PTFASZ as major structure active during the Early Palaeozoic evolution, being active only after Serpukhovian-Kasimovian (*c.a.* 318-308 Ma). According to these authors, the dextral ductile-brittle strike-slip kinematics that predominates at that time displaced older structures, like such as the TBCSZ and OMZ units, carrying his fragments towards the vicinity of Porto.

XIII.1.2.2. Variscan Deformation in Abrantes; Geometry and Kinematics

Some previous works consider the influence of the PTFASZ deformation in the Abrantes region negligible (Pereira *et al.*, 2010). However, recent studies (Moreira, 2012; Romão et al., 2014; Moreira et al., 2016; Fig. 1C) emphasize an important deformation related with this first order shear zone. Indeed, two major Variscan deformation phases have been reported for this region. The first one (D_1) generates NNW-SSE folds with a pervasive S_1 foliation developed at medium grade metamorphism, which often transpose bedding planes. Although there is a homogeneous orientation of the D_1 folds, their geometry is highly heterogeneous (Fig. 1C). In fact, an inner NNW-SSE sector with tangential transport towards NW (*i.e.* parallel to the orogenic trend) is bounded by two external domains with opposite vergences that are orthogonal to the strike of the main structures: at northeast the folds face NE while at southwest they face SW (Fig. 1C).

The D_1 structures are usually strongly deformed by a second deformation Variscan event (D_2) under a ductile to brittle-ductile regime. Such deformation is associated with an important dextral righ-lateral kinematics subparallel to previous main structures that often have been reworked during D_2. The geometry and kinematics of the D_2 structures are highly heterogeneous in the Abrantes region, due to the strong influence of previous fabrics. Nevertheless, the dextral D_2 NNW-SSE strike-slip component is always present as shown by a diversity of structures, like the frequent asymmetric boudins with subvertical necks affecting D_1 quartz veins. Associated to dextral pervasive kinematics two different styles of D_2 folding are found, often developed in adjacent domains:

- Tight to isoclinal orthorombic folds of previous planar fabrics, with subvertical axial planes and sub-horizontal to low dipping hinges (<10º). Locally, a slightly penetrative axial planar S_2 cleavage is found;
- Monoclinic folds with E-W subvertical axial planes and strongly plunging hinges (Fig. 1C). Such folds have usually en-echelon geometry in relation to the main shear enhancing the dextral kinematics. The interference with the major NW-SE D_1 folds gives rise to a macroscopic type 3 fold interference patterns (Ramsay, 1967).

XIII.1.2.3. D_2 Variscan Deformation in Abrantes; Geodynamical Evolution

The juxtaposition of domains with very different D_2 fold styles (Moreira, 2012), which are always coupled with the pervasive coeval dextral kinematics, indicates a strong strain partitioning in a general D_2 dextral transpression regime. The domains where the E-W to NW-SE D_2 monoclinic asymmetric folds with plunged hinges are dominant enhance a simple shear dominated transpression (according to Fossen *et al.*, 1994 nomenclature), where the NNW-SSE orthorhombic folds with low dipping hinges have been produced in a pure shear dominated transpressive regime. The boundaries between such domains are major D_2 dextral shear zones. Similar behaviour, with domains exhibiting pure-shear and simple shear dominated regimes, is well known and described by several authors at transpressive regimes with highly strain partitioning (e.g. Tikoff and Teyssier, 1994; Dias and Ribeiro, 1994; 2008; Fossen and Tikoff, 1998; Dias et al., 2003; Weinberger, 2014).

The existence of dextral kinematical markers ranging from ductile to brittle regimes seems to indicate that the dextral shearing along the NNW-SSE trend was a long lasting D_2 process. In the Abrantes region, the intensity of the D_2 deformation increases westwards in the direction of the PTFASZ (Moreira et al., 2016), which shows that D_2 Variscan deformation was induced by the activity of this dextral first order transcurrent shear.

XIII.1.3. The Abrantes Local Strike-Slip Domino

One of the major D_2 Abrantes NNW-SSE dextral shear zones makes the boundary between a limestone and a felsic volcano-sedimentary unit (Figs. 2A; Moreira, 2012). The felsic volcano-sedimentary unit has been strongly deformed by D_1, generating a penetrative subvertical NNW-SSE foliation (S_1) that often transpose bedding (N27ºW, 84ºNE; Fig. $2C_1$). In the S_1 plane is observed a stretching lineation (X_1) with very low plunges towards NNW, being subparallel to the regional L_1 intersection lineation (Fig. $2C_2$ and $2C_3$). Monoclinic and orthorhombic D_2 mesoscopic folds are common, sometimes with the local development of a slightly penetrative S_2 cleavage (N43ºW, 75ºE), mainly in the more pelitic layers (Fig. $2C_4$ and 3). The D_2 axial planes are subvertical and their trends range from E-W in the lower deformed domains, to NW-SE in the more deformed ones. The orientation of the fold hinges shows a strong dispersion induced by the interference with the D_1 structures (Fig. $2C_5$).

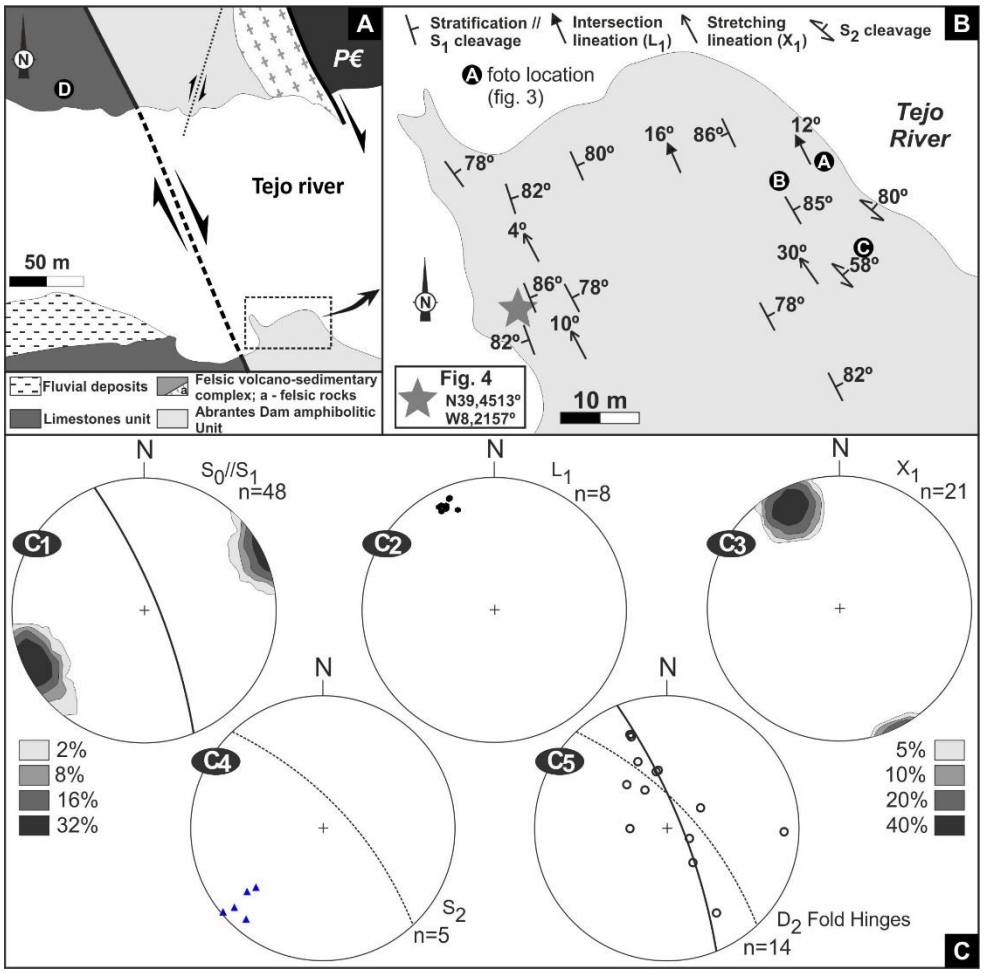

Figure 2 – Structural framework of Abrantes Domino region:

A – General Variscan structural map;

B – Structural detail in the vicinity of the domino outcrop;

C – Equal area lower hemisphere stereographic projections of main structures.

The angular relation between the E-W to NW-SE axial planes and the NW-SE S_2 cleavage with the NNW-SSE D_2 shear zones (N20ºW a N30ºW), indicates the *en-echelon* pattern expected in a D_2 regional dextral wrenching regime (Figs. 3A an 3B). Such non-coaxial dextral shearing is supported by a great diversity of D_2 structures, including folds asymmetry induced by the D_2 dextral centimetric to decametric 2nd order shear zones, associated to *en-echelon* behaviour of the D_2 minor folds (Figs. 3A an 3B), angular relation between the S_2 cleavage and the adjacent shear zones (Figs. 3C), sigmoidal bodies and shear bands (Fig. 3D).

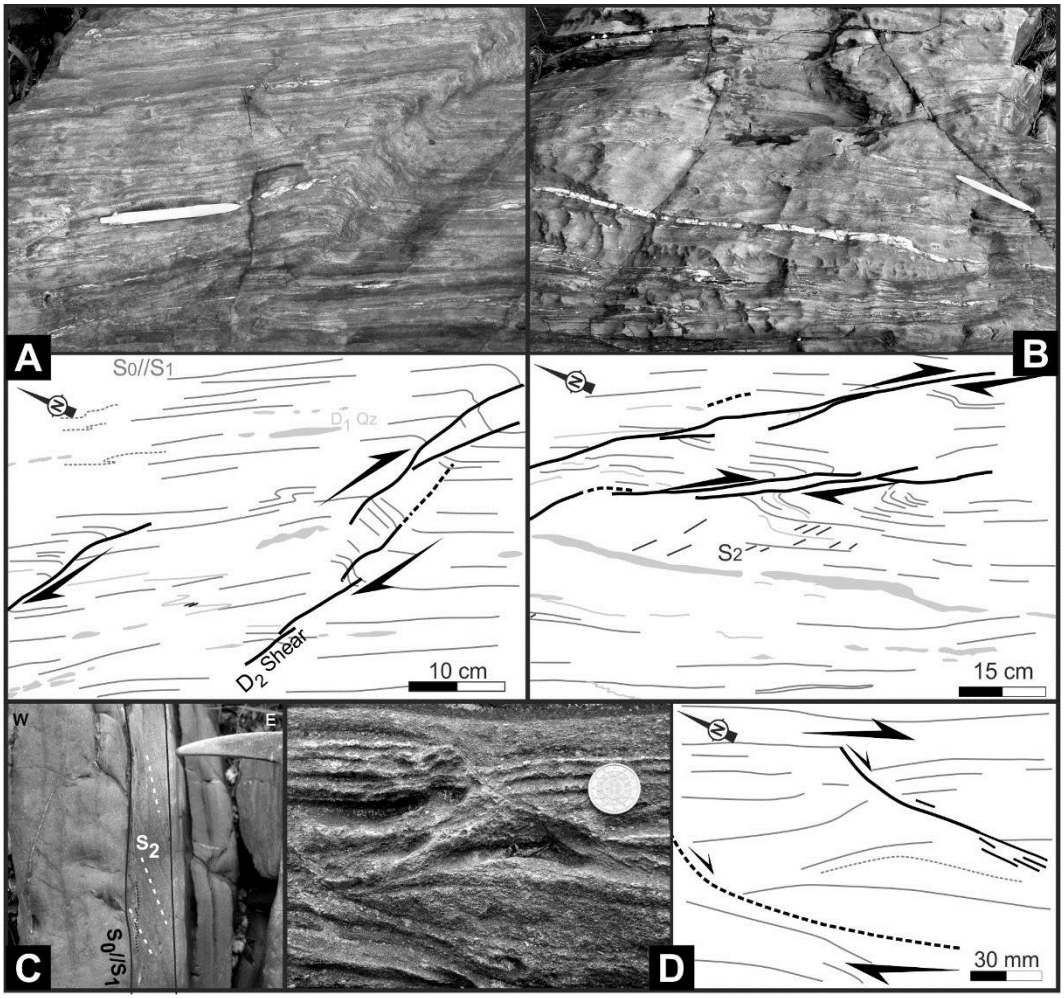

Figure 3 – Kinematical markers of D_2 dextral shearing:

A and B – Asymmetry of en-echelon D_2 minor folds associated to dextral shear bands;

C – Angular relation between S_2 and shear zones subparallel to $S_0//S_1$ layering;

D – Dextral Shear bands developed in the Limestone Unit, near the main shear zone.

In the felsic volcano-sedimentary unit, the dextral D_2 shearing give rise to a localized complex fracture pattern (Fig. 4A), strongly controlled by the decimetric silicate-rich layer, with millimetric to centimetric lamination. Such layering results from the transposition of the

stratification (S_0) by a S_1 cleavage (S_0 // S_1). The understanding of the evolution of this complex structure, where different shear zone families could be individualize (Fig. 4B), is the main aim of this work.

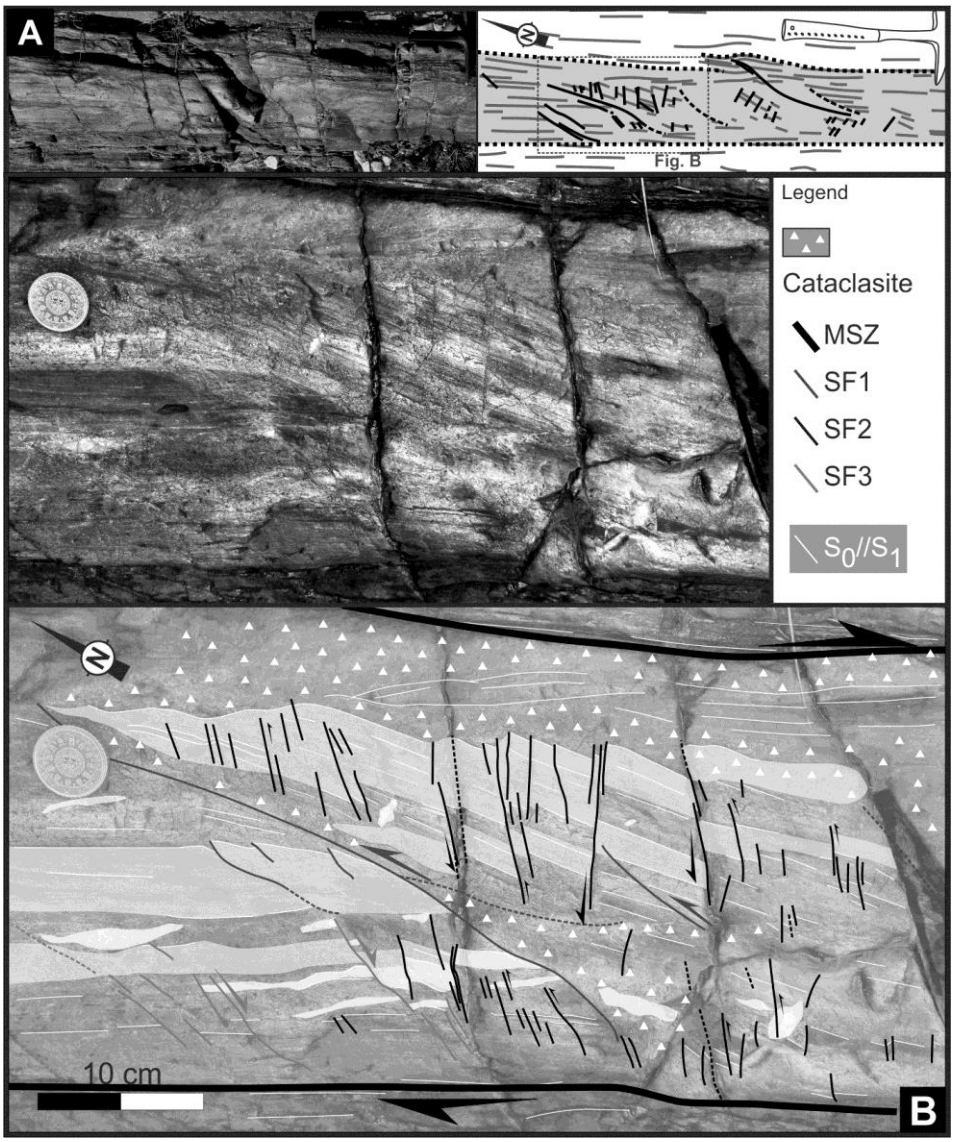

Figure 4 – Studied fracture pattern of Abrantes:

A – General pattern, showing the development of a heterogeneous fracture pattern;

B – Detail of figure A, enhancing the main structural pattern with discrimination of several shear families.

XIII.1.3.1. Geometrical and Kinematical Characterization

The complexity of the fracture pattern of Abrantes is due to the coexistence of several planar structures that accommodates the local stress within the shear zone (Fig. 4). As the layering is subvertical and the outcrop developed in a subhorizontal plane, the observed displacements along the individual shear zones are representative of horizontal offsets. This

does not preclude the existence of any subvertical component of movement, although it should be very small, because there is no evidence of such displacement has been found.

The fracture pattern has a localized development, being restricted to a decimetric domain bounded by NNW-SSE subvertical shear zones (MSZ). Such shears result from the reactivation of previous layering (S_0 // S_1) and act as a rigid barrier to the other shear zone families' propagation (Fig. 4), which were formed in its dependence.

The dextral movement along the MSZ during the D_2 regional event gives rise to a complex deformation of the inner domain, where the distortion, rotation and translation of several small blocks are common. These blocks are individualized by a numerous array of centimetric to decimetric shear zones. The exhibit fracture pattern could be considered divided in three main families according to their geometric and kinematics behaviour (Table 1; Fig. 5A).

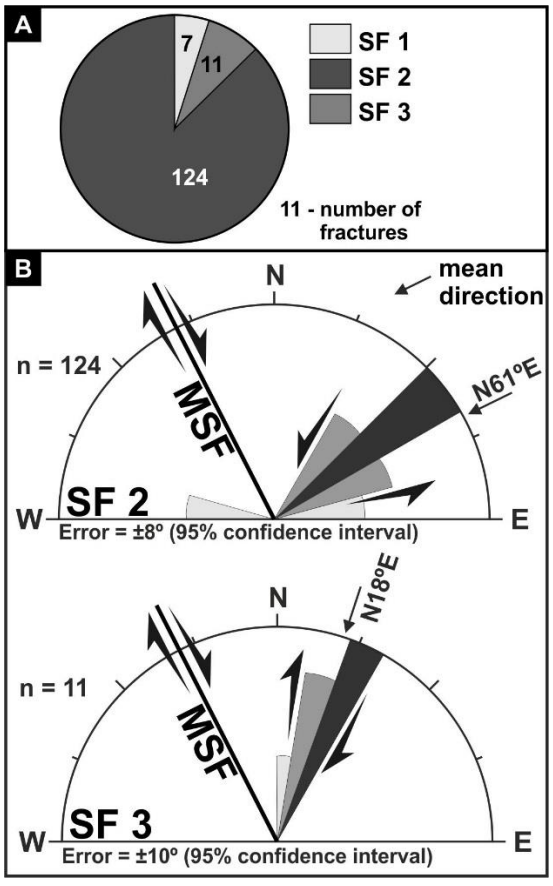

Figure 5 – Statistical analysis of the orientation of the shear zones orientations:

A – Relative distribution of shear zones family by number;

B – Variability of SF2 and SF3 orientations.

Table 1 – Geometric and kinematic features of Abrantes fracture pattern.

	Actual shear family main direction	Kinematics	Rotation of blocks	Cataclasis associated
MSZ	N27ºW	Dextral	No	Yes
SF1	N14ºE	Sinistral	No	Yes
SF2	N15ºE to S75ºE	Sinistral	Yes	No
SF3	N18ºE	Dextral	No	No

Shear Family 1 (SF1)

They are subvertical with a trend ranging from NNE-SSW to N-S direction (average orientation N14ºE, subvertical). They show a 45º mean angle to the MSZ, which tend to decrease when approaching the shear zone boundaries (FIG. 4B), that blocks its propagation. Although these discontinuities are not common when compared to other shear zone families (Fig. 5A, 6A and B), they have a large lateral continuity (Fig. 4), making them inescapable in any model that tries to explain the general pattern. The displacement induced by them in the regional $S_0//S_1$ layering enhance a sinistral kinematics (Fig. 6C), although in most continuous shears the kinematics is more dubious due to an intense cataclasis.

Shear Family 2 (SF2)

The SF2 shear zones are the most abundant family (Fig. 5A), individualizing several millimetric to centimetric blocks (Fig. 4B and 6A). These blocks exhibit a clear clockwise rotation, expressed by the angle between the $S_0//S_1$ layering inside the blocks and the regional layering, which is subparallel to MSZ (Fig. 4B). This rigid spinning always exhibits a clockwise sense, inducing a sinistral kinematics in the SF2 shears (Fig. 6A). However, the rotation angle between the blocks is not constant (see below), giving rise to a large dispersion in the trend of the planar structures belonging to this family (ranging between N15ºE and S75ºE, with a predominance of N60ºE direction; Fig. 5B). Nevertheless, the SF2 always exhibit a high angle to the MSZ general trend.

It is important to emphasize that this family has not a uniform distribution in the studied domain, being spatially restricted to SF1 and MSZ surrounding sectors (Fig. 4B and 6A). Therefore, these structures should have been dynamically related to the MSZ and SF1 activity.

Shear Family 3 (SF3)

The SF3 has an occasional development, appearing only in the marginal sectors of the area bordered by MSZ and SF1 (Fig. 4A and 6B), where the complex planar fabric is well marked and the SF1 and SF2 structures are predominant (Figs. 4B). It is characterized by dextral N-S to NNE-SSW shears (average direction N18ºE; Fig. 5C) and does not induce any rotation of blocks. This family appears to play a minor role in the observed pattern and in its dynamics.

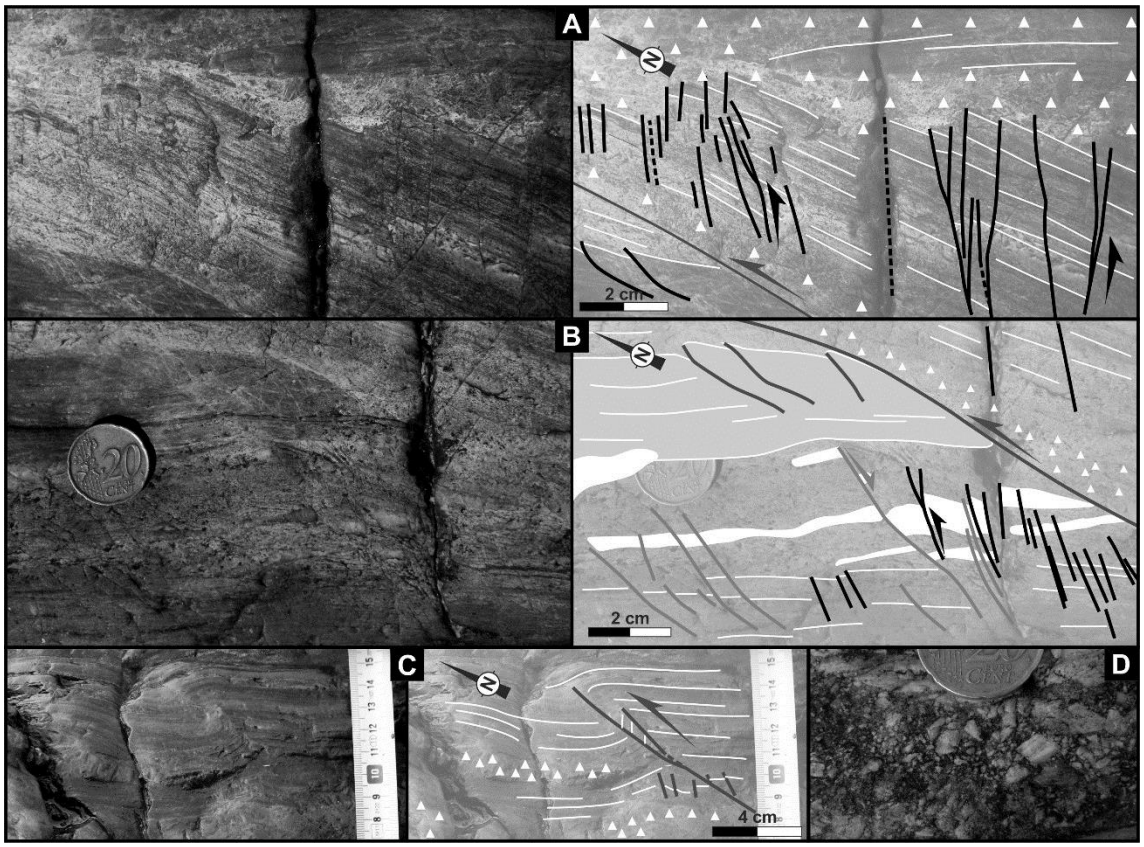

Figure 6 – Detailed geometric and kinematic features of the studied outcrop:

A – MSZ, SF1 and SF2 pattern, showing the presence of cataclasis associated to MSZ and SF1 shears and the rotated blocks bounded by SF2;

B – SF1 main shear ant its geometrical relation with the dominoes development domain, also showing the relation with dextral SF3;

C – Sinistral kinematics of SF1 structure;

D – Cataclasite associated to MSZ.

XIII.1.3.2. Rotational and Translational Characterization

Assuming fixed boundaries for the studied Abrantes shear zone, in a simple (or quasi-simple) shear mechanism, the rigid rotation of the domino blocks bounded by SF2 generates overlaps and gaps (Fig. 7). Such process could induce the formation of cataclasites, either in brittle, or in brittle-plastic transition (Engelder, 1974; Sibson, 1977; Ismat, 2006). In Abrantes shear zone the cataclasites are characterized by angular centimetric to millimetric lithoclasts, making difficult the distinction by simple mesoscopic observation between thin-crashed matrix and the larger centimetric fragments that compose the cataclasite (Fig. 6D).

Cataclastic flow, which accommodates ductile deformation in elastico-frictional regime (Sibson, 1977; Ismat, 2006), is located near the MSZ and SF1 shear zones (Figs. 4B, 6A and 6B), defining crushed zones. Such zones are characterized by distributed fracture and grain size

reduction throughout these families. Therefore, the blocks bounded by SF2 have a heterogeneous flux, with rigid (or quasi rigid) rotation, in a plastic matrix (constituted by cataclasite), which accommodates the overlaps and gaps created due the shear zones activity. The rigid block rotation, with no internal deformation, bounded by static boundaries generated in a simple shear regime are commonly named rigid-domino model (see Walsh and Watterson, 1991, Fossen and Hesthammer, 1998 and Fossen, 2010 references therein). However, in this model the planar structures that bound the blocks must exhibit constant rotation, strain rate, offsets and orientation, being parallel to each other, which was not observed in the study case (see discussion below).

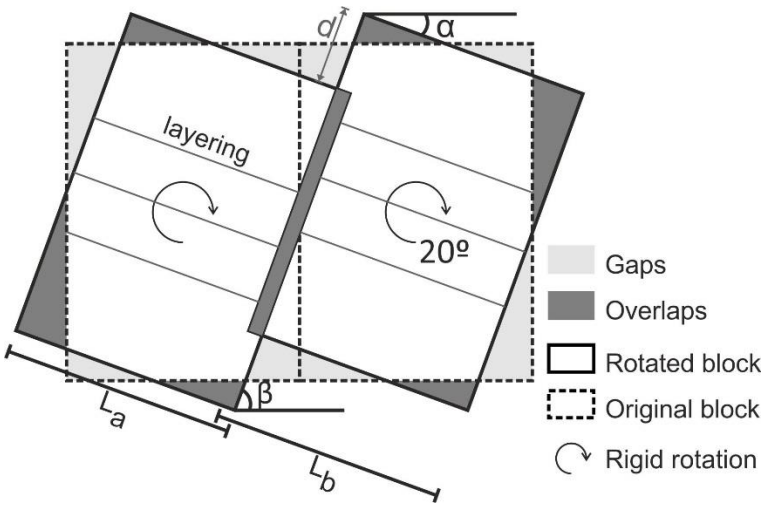

Figure 7 – Space problems induced by rigid block rotation and main geometrical parameters used in this study.

XIII.1.3.2.1. The Initial Angles; a Geostatistical Approach

A detailed analysis of the geometrical parameters related with block rotation in the Abrantes shear zone allowed the calculation of the initial angles between MSZ and SF2. These values are essential to establish the genetic relationships between the different shear zone families. Two angular parameters have been used: α (angle between the MSZ and S_0 // S_1 layering within blocks) and β (angle between the MSZ and SF2; Fig. 7). If the block rotation is totally rigid, these parameters should correlate; if the value of α increases, the β angle should decrease proportionately, in equal value. Therefore, the sum of the two angular parameters can provide an insight into the initial angle (β_0) of SF2 structures and its dispersion:

$$\beta_0 = \beta + \alpha$$

For the initial statistical analysis of β_0 population (n=121), it was used a box-plot graphic. The calculation of several statistical parameters of the β_0 population (*e.g.* median, quartiles,

maximum and minimum non-outliers) shows the presence of two outliers that deviate significantly from the general set (Fig, 8A$_1$). This analysis also shows that 50% of the data range between 107º and 120º values, with a median value of 115º. To minimize the errors, the two β_0 outliers (which could result either from sample variability, errors in the data collection or complex dynamic evolution) were not considered in the remaining statistical analysis.

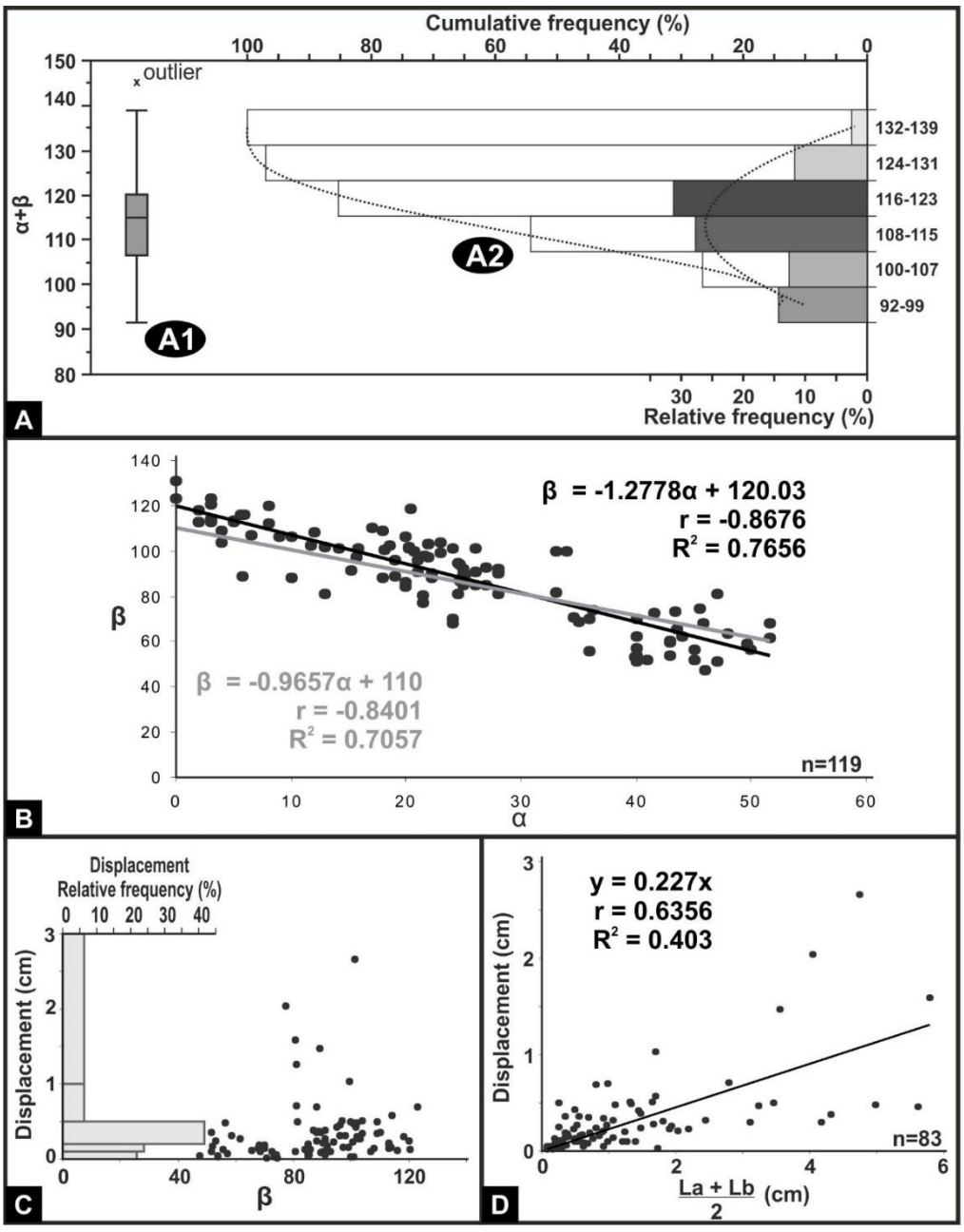

Figure 8 – Statistical analysis of the geometrical parameters of dominoes rotation shown in figure 7:

A – Variability of the β_0 data;

B – Correlation between α and β parameters;

C – Relation between the β parameter and the induced offset of adjacent blocks;

D – Relation between the offset between adjacent blocks and their wide.

The dataset, without outliers (n = 119), was projected in a histogram with six classes of seven degrees interval (Fig. 8A_2). To create representative statistical classes, it was used the Sturges' formula (valid for n <200). The histogram shows a data distribution close to a normal distribution, which was validated using the Kolmogorov-Smirnov test (*p-value*=0,36 to a 95% significance), with 59% of the data shared between the two central classes (106-115º and 116-123º). This indicates that the initial orientation of SF2 shears was not uniform, although there is a clear predominance (more than 50%) of β_0 values between 106º and 123º, which was also emphasized by the box-plot diagram.

In order to estimate the applicability of the theoretical model (Fig. 7) to the Abrantes dominoes, the correlation between α and β angular parameters was investigated (Fig. 8B). The obtained data show a strong negative linear correlation (Pearson's correlation coefficient r = -0.8676):

$$\beta = -1.2778\alpha + 120.03$$

The coefficient of determination (R^2) shows that 77% of β data (dependent variable) can be explained by a corresponding α (independent variable) variation of rigid blocks, as anticipated in initial assumption. This enables to estimate a mean angle of 60º between the shear zones that limit the blocks (SF2) and the main trend of the dextral shear (MSZ). Indeed, when the $S_0//S_1$ layering is parallel to the MSZ (*i.e.* when α =0º) the coeval β is 120º.

Nevertheless, the slope value obtained for this linear correlation (1.2778) slightly deviates from the value of 1.0 expected for a rigid rotation without internal deformation. Instead, if an initial value of 110º for SF2 is assumed, the coefficient of determination is slightly lower (R^2=0.7057), but the correlation between angular variables remains strong (Fig. 8B). In this case, the value of the slope strongly approaches the unit (0.9657). This seems to indicate that the initial acute angle between MSZ and SF2 families ranges between 60 and 70º.

The correlation between the angular parameters and the offsets of adjacent blocks (d parameter in Fig. 7) shows a random dispersion of data with no simple correlation (see Fig. 8C for a β parameter example). This seems to indicate the existence of other criteria controlling the offsets. Clearly the width of the blocks bounded by SF2 is one of the main factors which influence the offset between blocks. As the width of the left block (L_a) and he right one (L_b) equally affects the shear displacement (Fig. 7), any study of the offsets induced by domino rotation should use a mean block width:

$$\frac{L_a + L_b}{2}$$

The correlation between this parameter and the corresponding offsets should have a linear trend crossing the plot origin, because if the block width tends to zero, so does the offset. When

such approach is applied to Abrantes data (Fig. 8D) a moderate positive correlation is obtained (Pearson's correlation coefficient r = 0.6356), indicating that wider blocks induce bigger offsets. Nevertheless, the low value of the coefficient of determination (R^2 = 0,403) indicates that the width of the blocks could not be the only parameter affecting the offsets between adjacent blocks, because only 40% of the data could be explained by such correlation. This is not unexpected, because as α and β angular parameters also influence the offsets. Blocks with different spins must have different offsets.

The figure 8D diagram also shows the presence of some offsets well above the obtained correlation. Such anomalous values could have been influenced by a later reworking of SF2 shear zones. Moreover, the heterogeneous internal flow in the main shear zone could give rise to differential offsets along the SF2 shear planes, which will be independent of the offsets directly related to the domino rigid rotation. This additional movement could also explain the observed anomalous values.

XIII.1.3.2.2. Rotation and Translation of Dominos Blocks

As most of the deformation in the Abrantes studied shear zone (Fig. 9A) was the result of a rigid clockwise rotation between blocks, it is possible to restore the pre-deformation initial stage by the connection of homologous points of $S_0//S_1$ layering (Fig. 9B). This process allows estiating, not only the trajectories of the deformation, but also the shortening associated with heterogeneous deformation (next section). This restoration could confirm the previous statistical analysis.

The spatial analysis of isolated block rotation through pairs of homologous particles indicate a slightly differential spinning component between blocks (ranging from 13-14º to 20-23º; Fig. 9C). This variation is not random because the blocks in the vicinity of the SF1 shear zones have been less rotated. This shows the strong influence of this family in the deformation process.

Finite deformation pattern was obtained by two different methods. In the first one, the initial (Fig. 9B) and the final (Fig. 9A) stages are overlap using a point (P) which is considered fixed, defined in the central region of the deformed area. Then, each pair of homologous points is joint by arrowed linear segments (Fig. 9D).

The obtained pattern is an efficient way to study the flow pattern related to the shear activity (Passchier and Trouw, 2005). The strong symmetry of the Abrantes pattern around *P* point, emphasize a clockwise rotational component of deformation, compatible with synthetic spinning induced by the regional dextral simple shear dominated component. When approaching the MSZ that bounds the studied sector, the flow trajectories become almost

parallel to them (Fig. 10). The differential spinning between blocks inside the shear zone is also evident, contrasting with the absence of rotation outside the domino domain.

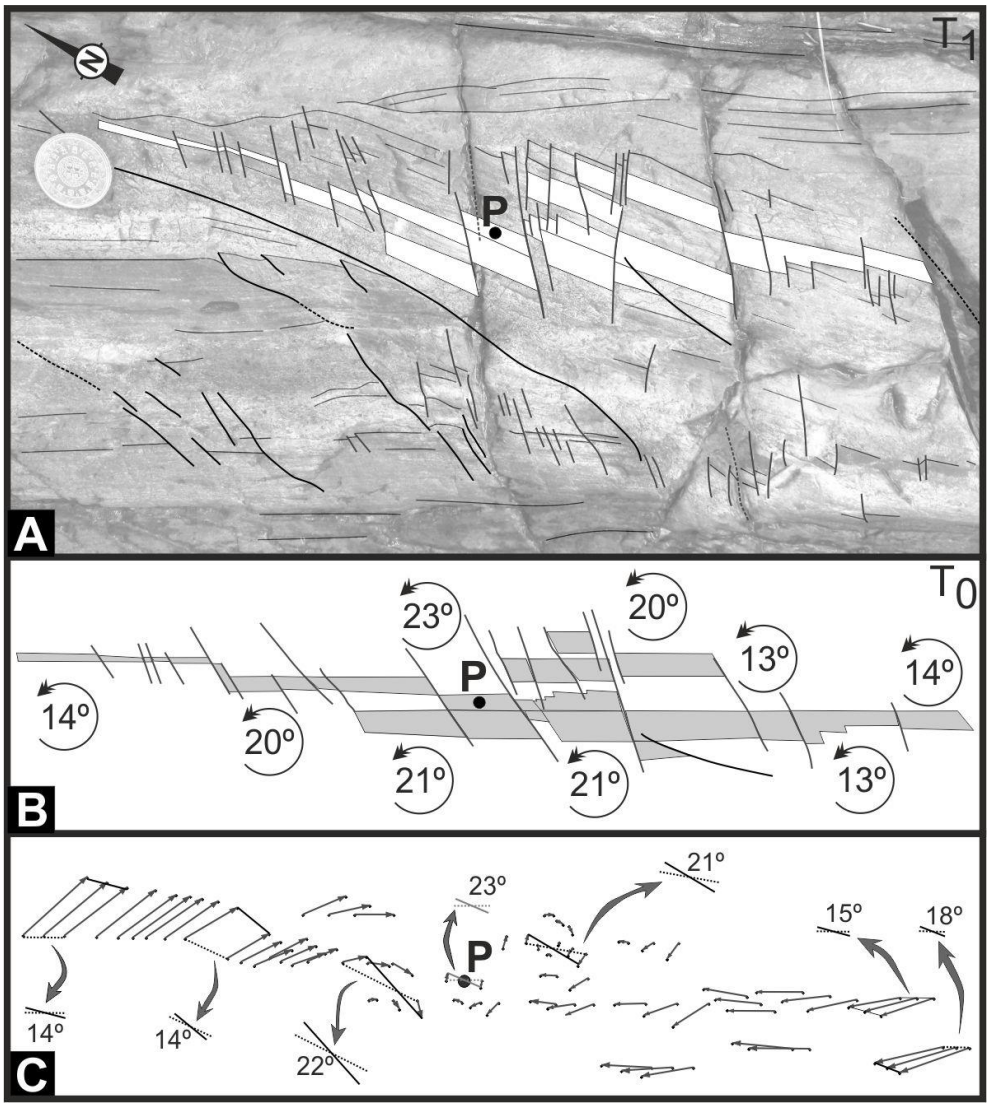

Figure 9 – Establishment of the deformation trajectories, using a central fixed point (P):

A – Final deformed stage;

B – Rigid block rotation restoration of the pre-deformation stage, with rigid rotation value used to restore the block early position;

C – Flow pattern induced by deformation, showing the individual particle rotation.

The second method (Fig. 10) intends to obtain the total displacement particle vectors during deformation. This pattern is generated by overlapping the final stage (Fig. 10A) and the pre-deformation one (Fig. 10B) using as a fixed point (P) located outside the domino domain. The obtained pattern (Fig. 9C) shows an important translational component induced by the overall activity of all shear zone families. The clockwise rotational component remains present,

although it is masked by the translational component related to SF1. This pattern is usually considered less useful (Passchier and Trouw, 2005), because some of the observed translation and rotation components have no geodynamical significance, masking the relative particle motion. Nevertheless, the strong parallelism between the general trajectories and the SF1 trend seems to confirm the important role of this family during deformation.

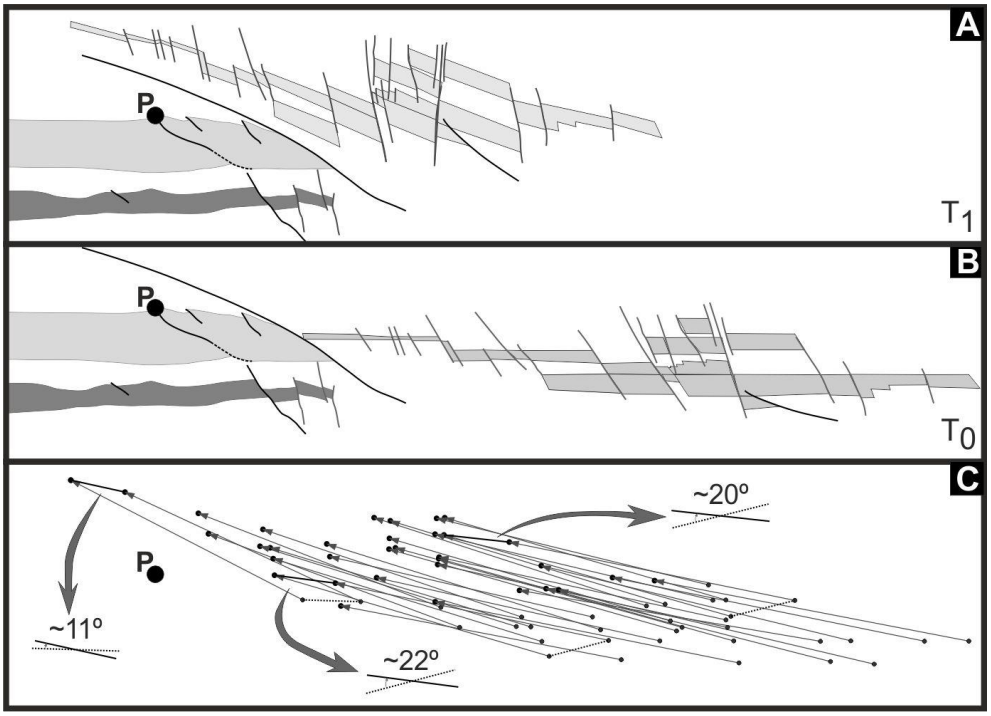

Figure 10 – Establishment of the deformation trajectories, using an outside fixed point (P):

A – Final deformed stage;

B – Restoration of the pre-deformation stage;

C – Flow pattern induced by deformation.

XIII.1.3.2.3. Quantitative approach to Deformation

Although the particle flow within the Abrantes domino has not been homogeneous due to the interaction between the several shear zones, two different geometrical approaches have been used to estimate the finite strain induced by the dextral shear deformation. In both cases, the final geometry (T_1 moment: Fig. 11A) is compared to the restore initial pattern (T_0 moment; Fig. 11B) which enables to quantify the stretch in homologous linear segments.

In the first method the stretch in three linear segments (lines A, B and C; Fig. 11) making high angles between them was obtained comparing their length in the deformed (L_1) and undeformed (L_0) states (Figs. 11A and 11B). When the stretches are known for any three different directions, the strain ellipse can be estimated (De Paor, 1988). The geometrical data

that have been used to estimate the finite strain using this approach, as well as the strain ellipse parameters, is resumed in table 2 and figure 11C. They show a moderate distortion (Rs=1,6) while the orientation of the ellipse is compatible with the dextral shearing along the MSZ.

As the three segments were chosen in order to enclose most of the domino domain, the obtained finite strain is representative of the deformation of the overall zone.

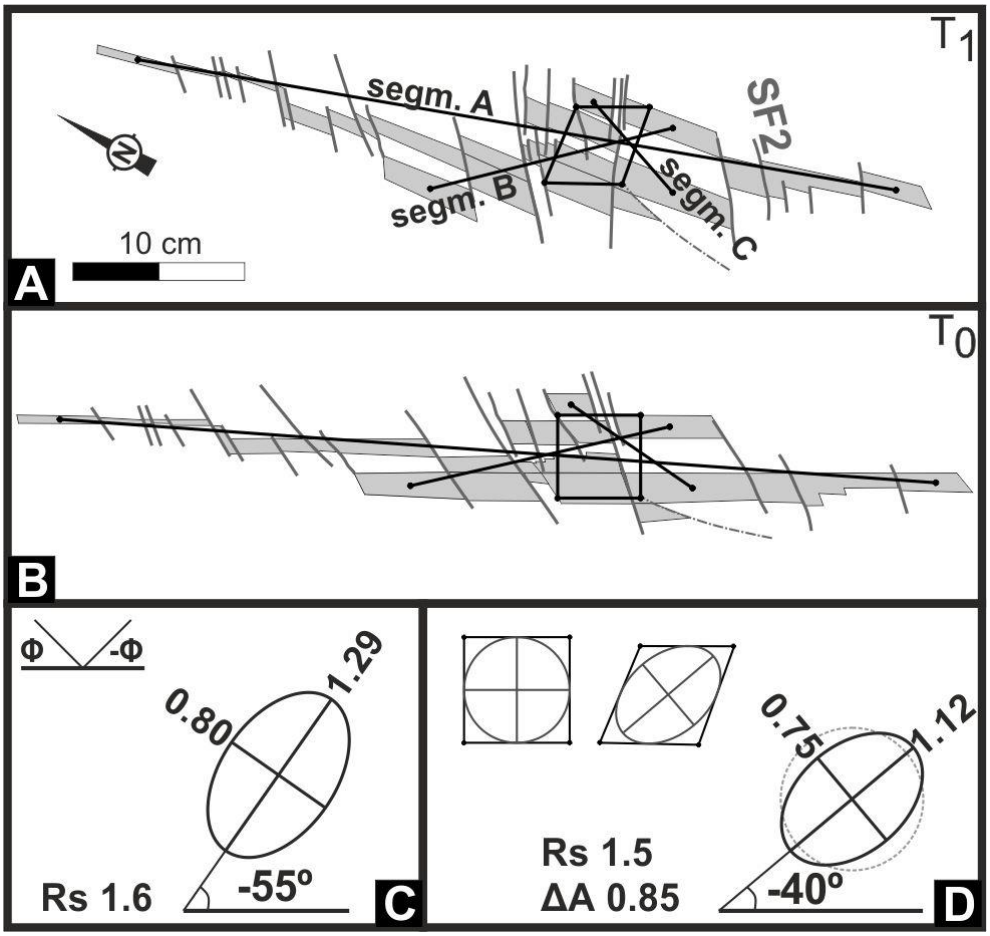

Figure 11 – Geometrical approach to estimate the finite strain in Abrantes shear zone:

A – Geometrical data in the final deformed stage that have been used;

B – Previous data restored to the pre-deformation stage;

C – Strain ellipse for the "three segments" approach;

D – Strain ellipse for the "square" approach.

The second method focus on the strain analysis in the inner zone of the Abrantes domino, where the block rotation has been greater (Fig. 9B and 9C). In this approach four points have been selected within the shear zone in the undeformed pattern, whose arrangement defines a square at T_0 moment (Fig. 11B). The same 4 corners of this square were identified in the deformed T_1 state, allowing to define a "rhombohedra" homologous of the previous square (Fig.

11A). A circumference was incircle in the undeformed square, while an ellipse was inscribed in the deformed rhombus (Fig. 11D). As the undeformed circle could be considered unitary, the ellipse represents the finite strain related to the distortion of the fabric. Table 3 and figure 11D synthesize the obtained strain parameters, which also show a moderate intensity (Rs=1,5) and also an orientation compatible with the dextral regional shear.

Table 2 – Strain data for the three studied segments.

		segment A	**segment B**	**segment C**
General trend		N20ºW	N44ºW	N29ºE
Angle to MSZ (φ)		6.7º	-17.1º	45.9º
Rotation		5.6º	1.4º	14.4º
L_0 (cm)		51.2	21.1	8.6
L_1 (cm)		44.9	22.4	7.0
Stretch ratio (L_1/L_0)		0.88	1.06	0.81
% shortening		12	-6	19
Strain ellipse	Major axis (s ; φ)	1.29 ; -55.1º		
	Minor axis (s ; φ)	0.80 ; 34.9º		
	Rs	1.6		

Table 3 – Strain data for "*square*" method.

	major axis	**minor axis**
General trend	N70ºW	N20ºE
Angle to MSZ (φ)	-40º	50º
L_0 (cm)	4.83	4.83
L_1 (cm)	5.43	3.64
Stretch ratio (L_1/L_0)	1.12	0.75
Shortening (%)	-12	25
Rs	1.5	
Δ area ($A_{ellipse}/A_{circle}$)	0.85	

As the strain ellipse was designed independently of the unitary circle, with this method it is also possible to estimate the area change induced by the deformation. The comparison between both areas indicates an area decrease of 15%. This decrease should be related with the space problems induced by the overlaps during block rotation. These problems led to material migration by cataclastic flow from the overlaps giving rise to the important concentration of cataclasites in the vicinity of the Abrantes shear zone boundaries (Fig. 4 and 6). Another possible explanation could be internal block deformation at the microscopic scale. Nonetheless**,** as previously mentioned, there is no mesoscopic evidence of internal deformation within blocks.

When comparing the finite strains estimated by both methods, although the approaches are strongly different, the results are rather similar. Indeed, not only the intensity of strain is comparable (1.5 and 1.6 strain ratios), but also both strain ellipses have major axes almost

parallel (-55º and -40º). This seems to indicate that even if the deformation inside the Abrantes shear zone could not be considered homogeneous, the heterogeneities are restricted.

XIII.1.4. Dynamic Processes and Genesis of Domino Structures; Discussion

The previous geometric and kinematic analysis of all shear zone families of Abrantes Domino, with special emphasis on SF2, allowed the perception of the genetic relations between them. The MSZ and SF1 clearly have a main role in the observed pattern, because they bound the domain where the rigid block rotation, circumscribed by SF2, is found, generating a domino structure.

The MSZ presents a right-lateral kinematics, while SF1 has an antithetic movement. The 45º acute angle between both families tends to decrease in the vicinity of the main shear zone boundary (Fig. 4B), where it can attain 25º. The reorientation of SF1 structures in the vicinity of MSZ could be the result of the reorientation of the local stress field induced by the movement along the previous $S_0//S_1$ anisotropy (Dyer, 1988), the drag of SF1 during MSZ activity or even of the internal material vorticity within the shear zone. In such context, important space problems should arise due to the interaction between these shear zone families, since the SF1 left-lateral displacements are blocked by the shear zone boundary (MSZ).

The sinistral kinematics of the SF2 family, which is antithetic to the general dextral shear (MSZ), indicates that they could be the result of a strike-slip domino mechanism. Similar behaviour has been proposed in Iberia for the Late Variscan deformation (Ribeiro, 2002; Dias et al., 2016a). The statistical analysis of the general orientation of SF2 (see section 3.1) seems to indicate it has genetic relation with SF1 family. As the initial acute angle between SF2 and MSZ (β0) usually ranges between 60 and 70º, the SF2 could be interpreted either as the sinistral conjugate of MSZ or R' shears (Logan *et al.*, 1992; Mandl, 2000; Brosch and Kurz, 2008). Thus, although the final geometry and kinematic of SF1 and SF2 are different, not only they could have been formed at the same time but, in the early stages, they were also sub-parallel.

It is now possible to present a model that explains the complex fracture pattern studied in the Abrantes shear zone (Fig 12).

In the early stages of D_2 deformation (T_0) the regional stress field induced the local reactivation of some previous major $S_0//S_1$ anisotropy as dextral shears (Fig. 12A). This reactivation was generated by a simple or quasi simple shear, which induces a non-coaxial internal deformation in the more competent layers of the Abrantes shear zone. The interference between closely spaced MSZ brittle-ductile shear zones could generate a dense fracture pattern of 2nd order shear zones oriented at 60º-70º to them (SF1 and SF2), with distinct spacing and size. Due to the highly non-coaxial deformation of Abrantes dextral shear zone and the

dispersion of the final trend observed in each family (see section 3.2.1), it is not easy to decide between a conjugated shear mechanism and the R´ one for such new shear zones. Whatever their initial origin, during the progression of deformation these new fractures could had different behaviours (Fig. 12B). The most continuous (SF1) interfere with the MSZ, bounding an inner high-strain domain, where the vorticity is stronger. Concerning the shorter shear zones (SF2) they rotated synthetically with the MSZ due to the overall vorticity, giving rise to an important rigid block spinning in a domino model. The space problems inside the Abrantes shear zone induced by this rigid rotation (Fig. 7) were partially solved by cataclasis, which removed material from the overlaps towards the local gaps, generating a cataclastic flow. This cataclastic flow also helps the rigid domino rotation, acting as a plastic matrix where the blocks could spin. A similar rigid block rotation in a plastic matrix has been described in asymmetric domino-like structures developed in high grade conditions (Goscombe and Passchier, 2003). Nevertheless, the quantitative approach using the "square" method shows a slightly area decrease (i.e. circa 15%) in the domino domain (Fig. 11D and table 3), which indicates that such flow could not be the only mechanism responsible to account for this geometrical problems.

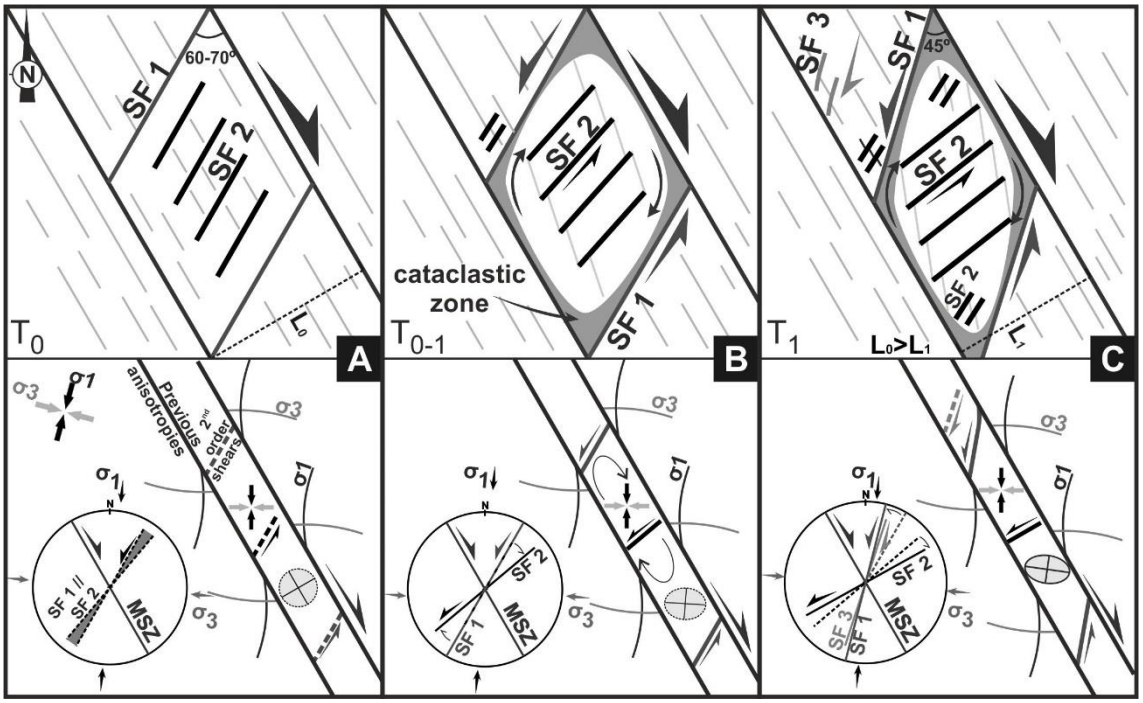

Figure 12 – Evolutionary proposal for the D_2 Abrantes shear zone.

A – Early stage of regional dextral shearing;

B – Major block rotation and coeval cataclastic formation;

C – Final rotation and shortening.

The rotation of R' structures during the progression of deformation is not uncommon (Mandl, 2000; Brosch and Kurz, 2008). Thus, although SF1 and SF2 have been subparallel in the early stages of D_2, their trend will diverge during the non-coaxial deformation. The continuity of D_2 dextral shearing (Fig. 12C), not only amplifies previous processes but also could induces the formation of new shear zones. This may explain the presence of small rotated narrow blocks inside the high strain zone, as well as the observed higher outlier's values. If it is considered a 2^{nd} generation of R' shears affecting a previously rotated layering, the α+β value does not represent the initial angle between MSZ and the SF2 (β_0), because α parameter is not equal to 0 when the new shear is created.

The geometry and kinematics of SF3 indicates they could be considered c' bands or Riedel shears of the D_2 MSZ dextral shear. Nevertheless, the angle between both families is slightly larger than what is expected for these structures (Mandl, 2000; Xypolias, 2010 and references therein). Such discrepancy could result from some orthogonal flattening during the late stages of D_2 deformation (Fig. 12C).

The proposed evolution has some discrepancies with the theoretical rigid-domino model (see Walsh and Watterson, 1991; Fossen and Hesthammer, 1998 for a discussion). Indeed, although the blocks have a rigid behaviour, there are some data which could not be explained:

- The SF2 are not perfectly linear, presents distinct sizes and present a range of general trends with an almost normal distribution around a mean value (Fig. 8A_2);
- The blocks present differential rotations, distinct sizes and consequently the shear zones present distinct offsets (Figs. 8D and 9);
- Although there is no evidence of internal mesoscopic deformation in the blocks, the finite strain analysis shows an area variation during the deformation process, suggesting an internal block deformation.

Previous data are more compatible with the so called soft-domino model (Walsh and Watterson, 1991; Fossen and Hesthammer, 1998). Yet, in the Abrantes domino, the blocks are more rigid than it was assumed by such model, which was possible due to the intense heterogeneous cataclastic flow, which acts as a matrix to the rigid block spinning that can generate the dissimilar rotations and offsets of SF2.

The strong non-coaxial deformation in the Abrantes shear zone, alongside the sin-kinematic synthetic rotation of earlier shear zones, give rise to a highly complex final pattern where the rigid block rotation is a crucial process in the fabric evolution.

XIII.1.5. Final Remarks

The studied Abrantes domino highlights:

- A close connection between the main dextral shearing and the clockwise synthetic rotation of domino structures, associated to a simple shear dominated transpression;

- A heterogeneous deformation, generating a complex pattern of shear structures;

- The presence of 2nd order shear zones, with antithetic kinematics (SF1), which together with the MSZ generates a clockwise internal flow within shear zone, is responsible by the rigid block spinning;

- The shear family that bounds the domino structures (SF2) could be formed as R' shears in initial stages, forming with an angle of 60-70º relatively to the MSZ;

- Although the deformation is highly heterogeneous, the finite strain data suggest the existence of a simple shear dominated transpression;

- The rigid block rotation was related to an intense cataclastic flow within the shear zone. The blocks have differential rotations and sizes, and consequently SF2 presents a distinct offset, compatible with the soft-domino model.

- Interpretation of domino structures, must be done carefully and its kinematic and dynamic analysis must to be supported by the general framework.

References

Axen, G.J. (1988). The geometry of planar domino-style normal faults above a dipping basal detachment. Journal of Structural Geology, 10, 405-411. DOI: 10.1016/0191-8141(88)90018-1

Bahroudi, A., Koyi, H. A., Talbolt, C. J. (2003). Effect of ductile and frictional décollements on style of extension, Journal of Structural Geology, 25, 1401–1423. DOI: 10.1016/0191-8141(88)90018-1

Brosch, F-J., Kurz, W. (2008). Fault damage zones dominated by high angle fractures within layer-parallel brittle shear zones: examples from the eastern Alps. In: Wibberley, C.A.J., Kurz, W., Imber, J., Holdsworth, R.E., Collettini, C (Eds.) The Internal Structure of Fault Zones: Implications for Mechanical and Fluid-Flow Properties, Geological Society, London, Special Publications, 299, 75–95. DOI: 10.1144/SP299.5

Chaminé, H. I., Gama Pereira, L. C., Fonseca, P. E., Noronha, F., Lemos de Sousa, M. J. (2003). Tectonoestratigrafia da faixa de cisalhamento de Porto–Albergaria-a-Velha–Coimbra–Tomar, entre as Zonas Centro-Ibérica e de Ossa-Morena (Maciço Ibérico, W de Portugal). Cad. Lab. Xeol. Laxe, A Coruña, 28, 37-78.

Cowan, D. S., Botros, M., Johnson, H. P. (1986). Bookshelf tectonics: Rotated crustal blocks within the Sovanco fracture zone, Geophys. Res. Lett., 13, 995-998. DOI: 10.1029/GL013i010p00995

Dabrowski, M., Grasemann, B., (2014). Domino boudinage under layer-parallel simple shear. Journal of Structural Geology, 68, 58–65. DOI: 10.1016/j.jsg.2014.09.006

De Paor, D. (1988). Strain determination from three known stretches. Journal of Structural Geology, 10, 639-642. DOI: 10.1016/0191-8141(88)90029-6

Dias, R., Ribeiro, A. (1993). Porto-Tomar shear zone, a major structure since the beginning of the Variscan orogeny. Comunicações do Instituto Geológico e Mineiro, 79, 29-38.

Dias, R., Ribeiro, A. (1994). Constriction in a transpressive regime: an example in the Ibero-Armoricain Arc. Journal of Structural Geology, (11), 1543–1554. DOI: 10.1016/0191-8141(94)90032-9

Dias, R., Ribeiro, A. (2008). Heterogeneous strain behaviour in competent layers during folding in transpressive regimes. Geodinamica Acta, 21(4), 219-229. DOI: 10.3166/ga.21.219-229

Dias, R., Mateus, A., Ribeiro, A. (2003). Strain partitioning in transpressive shear zones in the southern branch of the Variscan Ibero-Armorican Arc. Geodinamica Acta, 16, 119-129. DOI: 10.1016/j.geoact.2003.04.001

Dias, R., Moreira, N., Ribeiro, A., Basile, C. (2016a). Late Variscan Deformation in the Iberian Peninsula; A late feature in the Laurasia-Gondwana Dextral Collision. International Journal of Earth Sciences. DOI: 10.1007/s00531-016-1409-x

Dias, R., Ribeiro, A., Romão, J., Coke, C., Moreira, N. (2016b). A Review of the Arcuate Structures in the Iberian Variscides; Constraints and Genetical Models. Tectonophysics, 681, 170-194. DOI: 10.1016/j.tecto.2016.04.011

Dyer, R. (1988). Using joint interactions to estimate paleostress ratios. Journal of Structural Geology, 10, 685-699. DOI: 10.1016/0191-8141(88)90076-4

Engelder, J.T. (1974). Cataclasis and the generation of fault gouge. Geological Society of America Bulletin, 85(10), 1515-1522. DOI: 10.1130/0016-7606(1974)85<1515:CATGOF>2.0.CO;2

Figueiredo, R.P., Vargas, E.A., Moraes, A. (2004). Analysis of bookshelf mechanisms using the mechanics of Cosserat generalized continua. Journal of Structural Geology, 26, 1931–1943. DOI: 10.1016/j.jsg.2004.03.002

Fossen, H. (2010). Structural Geology. 1st Ed.. Cambridge University Press, 463 p.

Fossen, H., Hesthammer, J. (1998). Structural geology of the Gullfaks field, northern North Sea. In: Coward, M.P., Johnson, H., Daltaban, T.S. (Eds.), Structural Geology in Reservoir Characterization. Geological Society London Special Publication, 127, 231-261. DOI: 10.1144/GSL.SP.1998.127.01.16

Fossen, H., Tikoff, B. (1998). Extended models of transpression and transtension, and application to tectonic settings. In: Holdsworth, R.E., Strachan, R.A. and Dewey, J.F. (Eds.), Continental transpressional and transtensional tectonics. Geol. Soc. Lond. Spec. Publ., 135, 15-33. DOI: 10.1144/GSL.SP.1998.135.01.02

Fossen, H., Tikoff, B., Teyssier, C. (1994). Strain modeling of transpressional and transtensional deformation, Norsk Geologisk Tidsskrift, 74, 134–145.

Goscombe, B., Passchier, C.W. (2003). Asymmetric boudins as shear sense indicators – an assessment from field data. Journal of Structural Geology, 25(4), 575–589. DOI: 10.1016/S0191-8141(02)00045-7

Goscombe, B. D., Passchier, C. W., Hand, M. (2004). Boudinage classification: end-member boudin types and modified boudin structures. Journal of Structural Geology, 26(4), 739-763. DOI: 10.1016/j.jsg.2003.08.015

Iglésias, M., Ribeiro, A. (1981). Zones de cisaillement ductile dans l'arc ibéro-armoricain. Comunicações do Instituto Geológico e Mineiro, 67, 85-87.

Ismat, Z. (2006). Cataclastic flow: a means for ensuring ductility within the elastico-frictional regime. Geological Society of America Annual Meeting Abstract with Programs, 38 (7), 310.

Jaeger J.C., Cook N.G.W. (1987). Fundamentals of rock mechanics, 3rd ed., Chapman and Hall, London, 593 p.

Julivert, M., Fontbote, J. M., Ribeiro, A., Conde, L.E.N. (1974). Memória Explicativa do Mapa Tectónico da Península Ibérica Y Baleares, Escala 1:1 000 000, Inst. Geol. Min. España, 1-113.

Karlstrom, K.E., Heizler, M., Quigley, M.C. (2010). Structure and $^{40}Ar/^{39}Ar$ K-feldspar thermal history of the Gold Butte block: Reevaluation of the tilted crustal section model. In: Umhoefer, P.J., Beard, L.S., Lamb, M.A. (Eds.), Miocene Tectonics of the Lake Mead Region, Central Basin and Range. Geological Society of America Special Paper, 463(15), 331–352. DOI: 10.1130/2010.2463(15).

Karmakar, S., Mandal, N. (1989). Rotation and offset of shear fracture boudins. Indian Journal of Geology 61, 41-49.

La Femina, P.C., Dixon, T.H., Strauch, W. (2002). Bookshelf faulting in Nicaragua, Geology, 30, 751–754. DOI: 10.1130/0091-7613(2002)030<0751:BFIN>2.0.CO;2

Lefort, J.P., Ribeiro, A. (1980). La faille de Porto-Badajoz-Cordobe a-t-elle contrôlé l'évolution de lócéan paleéozoique sud-Armoricain?. Bull. Soc. Géol. France, 7, XXII (3), 455-462.

Logan J.M., Dengo C.A., Higgs N.G., Wang Z.Z. (1992). Fabrics of experimental fault zones: their development and relationship to mechanical behaviour. In: Evans B., Wong T.F. (Eds.), Fault mechanics and transport properties of rocks. International Geophysics, 51, 33-67. DOI: 10.1016/S0074-6142(08)62814-4

Lotze, F. (1945). Zur Gliderung der Varisziden in der Iberischen Meseta. Geotekt. Forsch., 6, 78- 92.

Mandal, N., Khan, D. (1991). Rotation, offset and separation of oblique-fracture (rhombic) boudins: theory and experiments under layer-normal compression. Journal of Structural Geology, 13, 349-356. DOI: 10.1016/0191-8141(91)90134-5

Mandal, N., Chakraborty, C., Samanta, S.K. (2000). Boudinage in multilayered rocks under layer-normal compression: a theoretical analysis. Journal of Structural Geology, 22(3), 373–382. DOI: 10.1016/S0191-8141(99)00156-X

Mandal, N., Dhar, R., Misra, S., Chakraborty, C. (2007). Use of boudinaged rigid objects as a strain gauge: Insights from analogue and numerical models. Journal of Structural Geology, 29(5), 759-773. DOI: 10.1016/j.jsg.2007.02.007

Mandl, G. (1984). Rotating Parallel Fault – "Book Shelf" Mechanism. American Association of Petroleum Geologists Bulletin, 68, 502-503.

Mandl, G. (1987). Tectonic deformation by rotating parallel faults: the "bookshelf' mechanism. Tectonophysics, 141 (4), 277-316. DOI: 10.1016/0040-1951(87)90205-8

Mandl, G. (2000). Faulting in brittle rocks: an introduction to the mechanics of tectonic faults. Springer-Verlag, Berlin. ISBN: 978-3-662-04262-5

Matte, P. (2001). The Variscan collage and Orogeny (480 – 290 Ma) and the tectonic definition of the Armorica microplate: A review, Terra Nova, 13, 122 – 128. DOI: 10.1046/j.1365-3121.2001.00327.x

Moreira, N. (2012). Caracterização estrutural da zona de cisalhamento Tomar-Badajoz-Córdova no sector de Abrantes. Unpublished MSc thesis, University of Évora, 225 p.

Moreira, N., Romão, J., Pedro, J., Dias, R., Ribeiro, A. (2016). The Porto-Tomar-Ferreira do Alentejo Shear Zone tectonostratigraphy in Tomar-Abrantes sector (Portugal). Geo-Temas, 16(1), 85-88. ISSN 1576-5172.

Moreira, N., Araújo, A., Pedro, J.C., Dias, R. (2014). Evolução geodinâmica da Zona de Ossa-Morena no contexto do SW Ibérico durante o Ciclo Varisco. Comunicações Geológicas, 101 (I), 275-278.

Nance, R.D., Gutierrez-Alonso, G., Keppie, J.D., Linnemann, U., Murphy, J.B., Quesada, C., Strachan, R.A., Woodcock, N.H. (2010). Evolution of the Rheic Ocean. Gondwana Research, 17, 194-222. DOI: 10.1016/j.gr.2009.08.001

Nance, R.D., Gutiérrez-Alonso, G., Keppie, J.D., Linnemann, U., Murphy, J.B., Quesada, C., Strachan, R.A., Woodcock, N.H. (2012). A brief history of the Rheic Ocean. Geoscience Frontiers, 3(2), 125-135. DOI: 10.1016/j.gsf.2011.11.008

Nixon, C. W., Sanderson, D. J., Bull, J. M. (2011). Deformation within a strike-slip fault network at Westward Ho!, Devon U.K.: Domino vs conjugate faulting. Journal of Structural Geology, 33, 833-843. DOI: 10.1016/j.jsg.2011.03.009

Passchier, C.W., Myers, J.S., Kröner, A. (1990). Field Geology of High-Grade Gneiss Terrains. Springer-verlag Berlin Heidelberg New York, 150 p. ISBN: 3-540-53053-3.

Passchier, C.W., Trouw, R.A.J. (2005). Microtectonics. 2nd Ed., Springer, New York, 382 p. ISBN 978-3-540-64003-5

Pereira, M.F., Silva, J.B., Drost, K., Chichorro, M., Apraiz, A. (2010). Relative timing of the transcurrent displacements in northern Gondwana: U-Pb laser ablation ICP-MS zircon and monazite geochronology of gneisses and

sheared granites from the western Iberian Massif (Portugal). Gondwana Research, 17, 461–481. DOI: 10.1016/j.gr.2009.08.00.

Ramsay, J.G. (1967). Folding and Fracturing of rocks. MacGraw Hill, New York, 568 p.

Ribeiro, A. (2002). Soft Plate and Impact Tectonics. Springer Verlag, Berlin, 324 p. ISBN: 978-3540679639

Ribeiro, A., Antunes, M. T., Ferreira, M. P., Rocha, R. B., Soares, A. F., Zbyszewski, G., Moitinho de Almeida, F., Carvalho, D., Monteiro, J. H. (1979). Introduction à la géologie générale du Portugal. Serviços Geológicos de Portugal, 114 p.

Ribeiro, A., Munhá, J., Dias, R., Mateus, A., Pereira, E., Ribeiro, M.L., Fonseca, P., Araújo, A., Oliveira, T., Romão, J., Chaminé, H., Coke, C., Pedro, J. (2007). Geodynamic evolution of SW Europe Variscides, Tectonics, 26(6). DOI: 10.1029/2006TC002058

Ribeiro, A., Munhá, J., Mateus, A., Fonseca, P., Pereira, E., Noronha F., Romão, J., Rodrigues, J. F., Castro, P., Meireles, C., Ferreira, N. (2009). Mechanics of thick-skinned Variscan overprinting of Cadomian basement (Iberian Variscides). Comptes Rendus Geoscience, 341 (2-3), 127-139. DOI: 10.1016/j.crte.2008.12.003

Ribeiro, A., Romão, J., Munhá, J., Rodrigues, J., Pereira, E., Mateus, A., Araújo, A. (2013). Relações tectonostratigráficas e fronteiras entre a Zona Centro-Ibérica e a Zona Ossa-Morena do Terreno Ibérico e do Terreno Finisterra. In: Dias, R., Araújo, A., Terrinha, P., Kullberg, J.C. (Eds.), Geologia de Portugal, vol. 1, Escolar Editora, 439-481. ISBN: 978-972-592-364-1

Romão, J., Coke, C., Dias, R., Ribeiro, A. (2005). Transient inversion during the opening stage of the Wilson Cycle "Sardic phase" in the Iberian Variscides: stratigraphic and tectonic record. Geodin. Acta, 18/2, 15-29.

Romão, J., Metodiev, D., Dias, R., Ribeiro, A. (2013). Evolução geodinâmica dos sectores meridionais da Zona Centro-Ibérica. In: Dias, R., Araújo, A., Terrinha, P., Kullberg, J.C. (Eds.), Geologia de Portugal, vol. 1, Escolar Editora, 206-257. ISBN: 978-972-592-364-1.

Romão, J., Moreira, N., Dias, R., Pedro, J., Mateus, A., Ribeiro, A. (2014). Tectonoestratigrafia do Terreno Ibérico no sector Tomar-Sardoal-Ferreira do Zêzere e relações com o Terreno Finisterra. Comunicações Geológicas, 101 (I), 559-562.

Scholz, C.H., Ando, R. Shaw, B.E. (2010). The mechanics of first order splay faulting: The strike-slip case. Journal of Structural Geology, 32, 118–126, DOI: 10.1016/j.jsg.2009.10.007

Shelley, D., Bossière, G. (2000). A new model for the Hercynian orogen of Gondwanan France and Iberia. Journal of Structural Geology, 22, 757–776. DOI: 10.1016/S0191-8141(00)00007-9.

Sibson, R.H. (1977). Fault rocks and fault mechanism. Journal of the Geological Society, London, 133 (3), 191-213. DOI: 10.1144/gsjgs.133.3.0191

Tikoff, B., Teyssier, C. (1994). Strain modeling of displacement-field partitioning in transpressional orogens. Journal Structural Geology, 16, 1575-1588. DOI: 10.1016/0191-8141(94)90034-5

Walsh, J. J., Watterson, J. (1991). Geometric and kinematic coherence and scale effects in normal fault systems. Geological Society, London, Special Publication, 56, 193-203. DOI: 10.1144/GSL.SP.1991.056.01.13

Weinberger, R. (2014). Pleistocene strain partitioning during transpression along the Dead Sea Transform, Metulla Saddle, northern Israel. In: Garfunkel, G., Ben-Avraham, Z., Kagan, E., (Eds.), Dead Sea Transform Fault System: Reviews, Chapter 6, Springer-Verlag, Heidelberg, 151-182. DOI:10.1007/978-94-017-8872-4_6.

Wernicke, B., Burchfiel, B.C. (1982). Modes of extensional tectonics. Journal of Structural Geology, 4(2), 105-115. DOI: 10.1016/0191-8141(82)90021-9

Xypolias, P. (2010). Vorticity analysis in shear zones: A review of methods and applications. Journal of Structural Geology, 32, 2072-2092. DOI: 10.1016/j.jsg.2010.08.009